

SUPPORTING INFORMATION

Ni@4H-Chromene based Core-Shell Nanoparticles: Highly Sensitive and Selective Chemosensor for Radiosensitizer - Bromodeoxyuridine

Geetika Bhardwaj,^a Randeep Kaur,^a Sanjeev Saini,^b Navneet Kaur,^a Narinder Singh^b

*^a Department of Chemistry & Centre for Advanced Studies in Chemistry, Panjab University,
Chandigarh 160014, India*

*^b Department of Chemistry, Indian Institute of Technology Ropar (IIT Ropar), Rupnagar,
Punjab 140001, India*

Table of Contents:

Fig. S1 A) DLS histogram of ONPs depicting average size of 44 nm. B) TEM images of ONPs showing spherical shaped particles.

Fig. S2 A) EDAX mapping of ONPs showing presence of carbon, nitrogen and oxygen. B) SEM image of receptor **G1** ONPs.

Fig. S3 A) Graph showing change in UV-Visible profile of ONPs on change in concentration of receptor **G1** solution. B) Fluorescence spectrum showing increases in fluorescence intensity on increasing receptor **G1** solution in ONPs. C) DLS showing variation in size of ONPs as a function of concentration.

Fig. S4 A) Spectrum showing no obvious change in emission profile of ONPs with thymidine analogs. B) Bar graph showing no specific interaction of ONPs with thymidine analogs.

Fig. S5 Fluorescence spectrum of binding studies of ONPs with various anions.

Fig. S6 A) Metal binding graph of ONPs showing selectivity towards Ni (II) ion. B) Bar graph showing selective bindings of ONPs with Ni (II). C) Spectrum showing changes in fluorescence emission profile on adding small aliquots of Ni (II). D) Linear regression plot from titrations of ONPs with Ni (II) ion showing linearity of 95%.

Fig. S7 Calibration plot of titrations of **G2** with BrdU A) UV visible B) Fluorescence C) Cyclic voltammetry.

Fig. S8 A) Fluorescence spectrum showing shift and enhancement in emission intensity of **G2** upon addition of BrdU. B) Bar graph showing selectivity of **G2** towards BrdU.

Fig. S9 A) Titrations of Ni complex in organic medium. B) Calibration plot of variation in fluorescence intensity on varying the concentration of BrdU.

Fig. S10 Effect of tetrabutylammonium A) perchlorate B) phosphate C) sulphate, on the fluorescence emission intensity of **G2**. D) Effect of increase in temperature from 25-105 °C on fluorescence emission intensity of **G2**. E) Fluorescence spectrum showing negligible change in emission intensity of **G2** on varying pH from 2-12.

Fig. S11 Zeta potential of A) ONPs and B) **Ni@G1** showing change in its surface charge upon coating.

Fig. S12 DLS of **Ni@G1** showing average hydrodynamic size of 92 nm.

Fig. S13 A) Circular dichroism showing changes in ONPs profile upon formation of **Ni@G1**.

Fig. S14 Calibrations plot showing dependence of BrdU addition on **Ni@G1** on Cyclic voltammetry.

Fig. S15 A) Cyclic voltammogram showing variation in current and potential on varying scan rate from 20 – 500 mV/s. B) Linear regression plot between log current versus square root of scan rate

Fig. S16 A) Changes in dextrorotatory behavior on adding small aliquots of BrdU to Ni@G1. B) Calibration showing linearity of 98.65% with BrdU concentration.

Fig. S17 A) Effect of tetrabutylammonium phosphate on the fluorescence emission intensity of Ni@G1 complexed with BrdU. B) Effect of temperature therapy from 25-105 °C on fluorescence emission intensity of Ni@G1 complexed with BrdU. C) Fluorescence spectrum showing negligible change in emission intensity of Ni@G1 complexed with BrdU on varying pH from 2-12.

Fig. S18: Plausible mechanism for the interaction of sensing.

Fig. S19: A) Cyclic voltammogram showing changes in cathodic and anodic peak when Ni(II) is added to ONPs. B) Cyclic voltammogram when NaBH₄ is added to the G2 complex formed.

Table S1 Time resolved fluorescence data of receptor G1, ONPs, G2 and Ni@G1.

Table S2 Comparison table of present work with other analytical techniques.

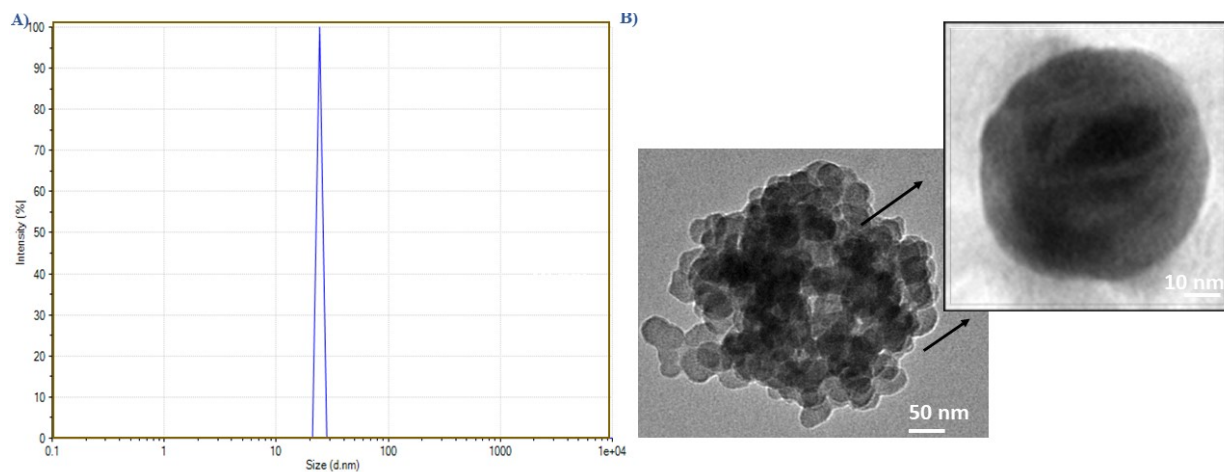


Fig. S1 A) DLS histogram of ONPs depicting average size of 44 nm. B) TEM images of ONPs showing spherical shaped particles.

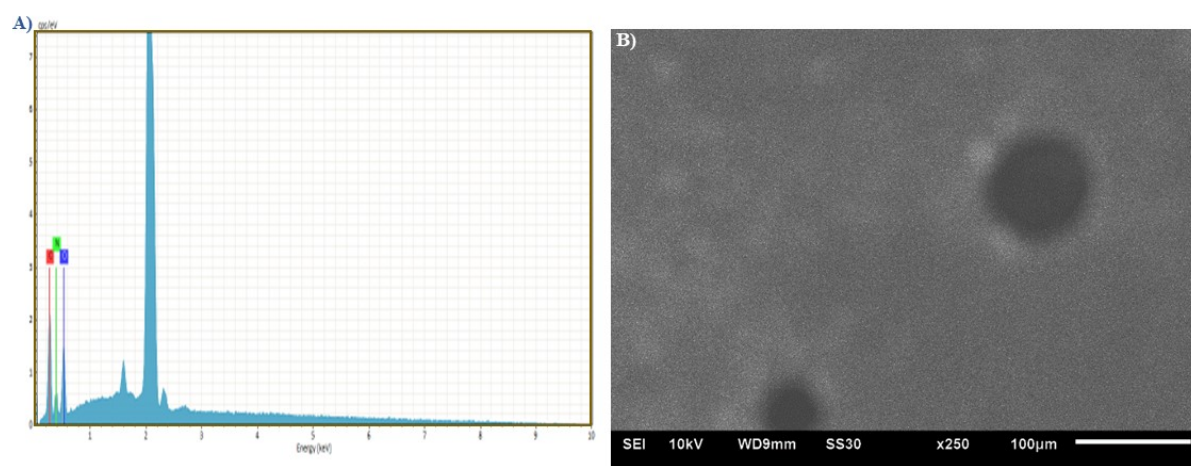


Fig. S2 A) EDAX mapping of ONPs showing presence of carbon, nitrogen and oxygen. B) SEM image of receptor **G1** ONPs.

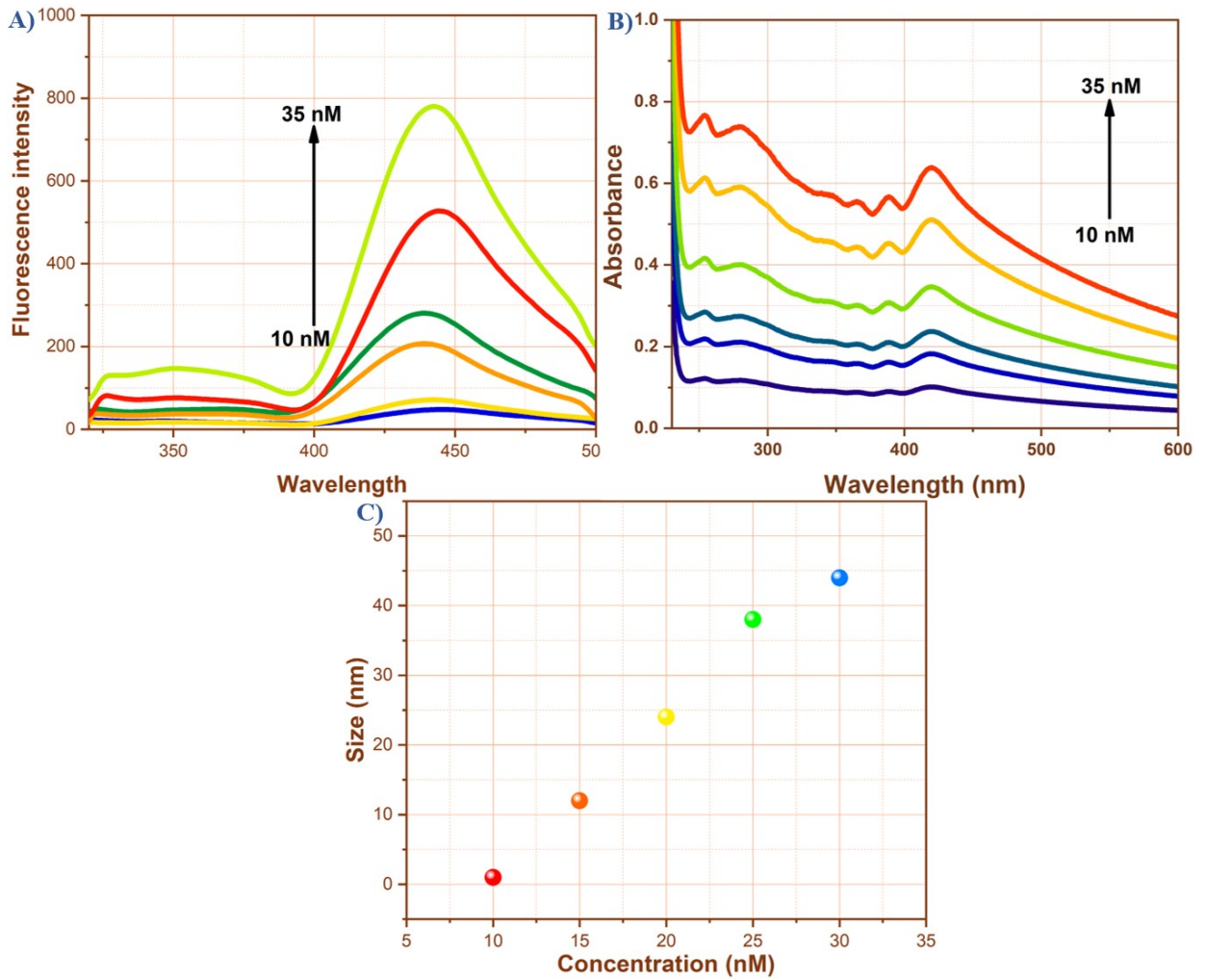


Fig. S3 A) Graph showing change in UV-Visible profile of ONPs on change in concentration of receptor **G1** solution. B) Fluorescence spectrum showing increases in fluorescence intensity on increasing receptor **G1** solution in ONPs. C) DLS showing variation in size of ONPs as a function of concentration.

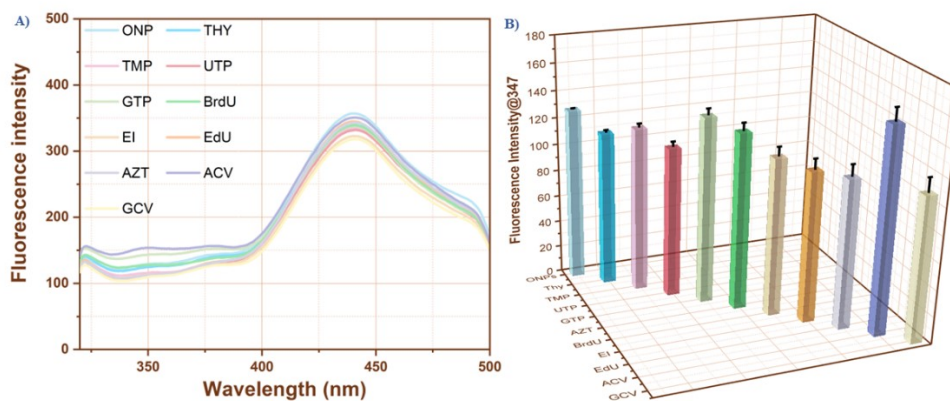


Fig. S4 A) Spectrum showing no obvious change in emission profile of ONPs with thymidine analogs. B) Bar graph showing no specific interaction of ONPs with thymidine analogs.

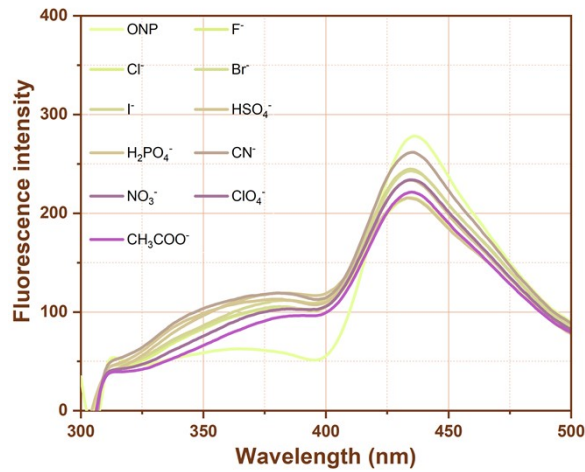


Fig. S5 Fluorescence spectrum of binding studies of ONPs with various anions.

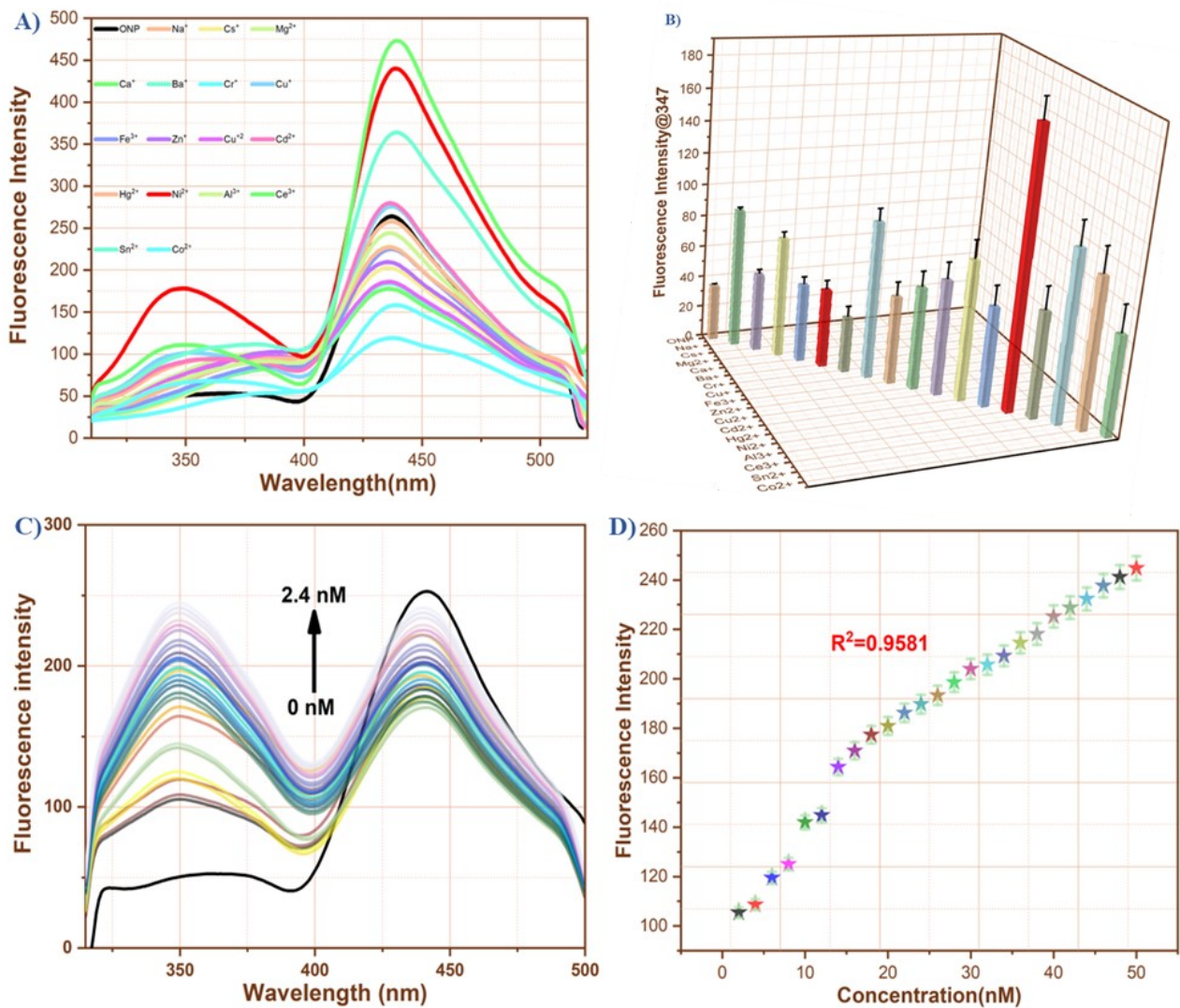


Fig. S6 A) Metal binding graph of ONPs showing selectivity towards Ni (II) ion. B) Bar graph showing selective bindings of ONPs with Ni (II). C) Spectrum showing changes in fluorescence emission profile on adding small aliquots of Ni (II). D) Linear regression plot from titrations of ONPs with Ni (II) ion showing linearity of 95%.

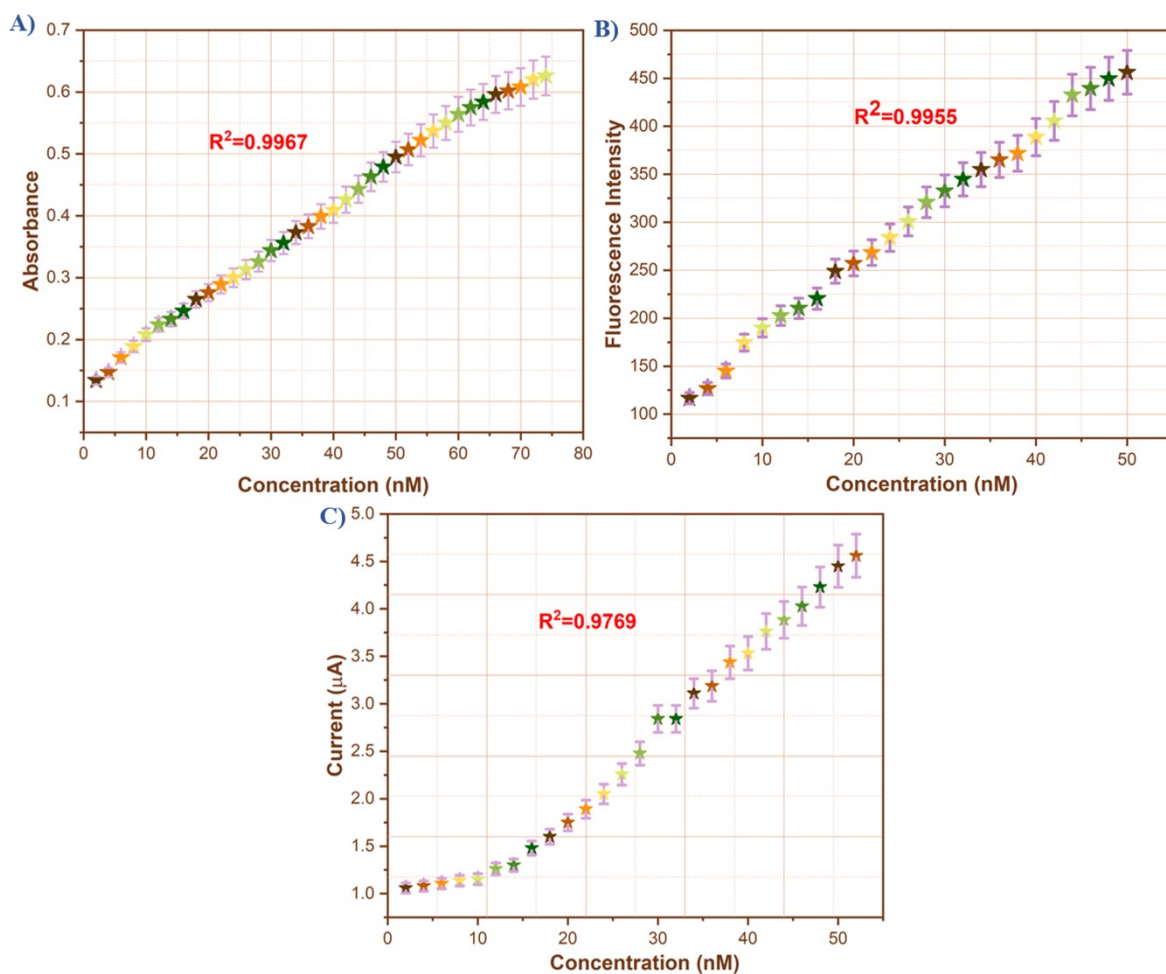


Fig. S7 Calibration plot of titrations of **G2** with BrdU A) UV visible B) Fluorescence C) Cyclic voltammety.

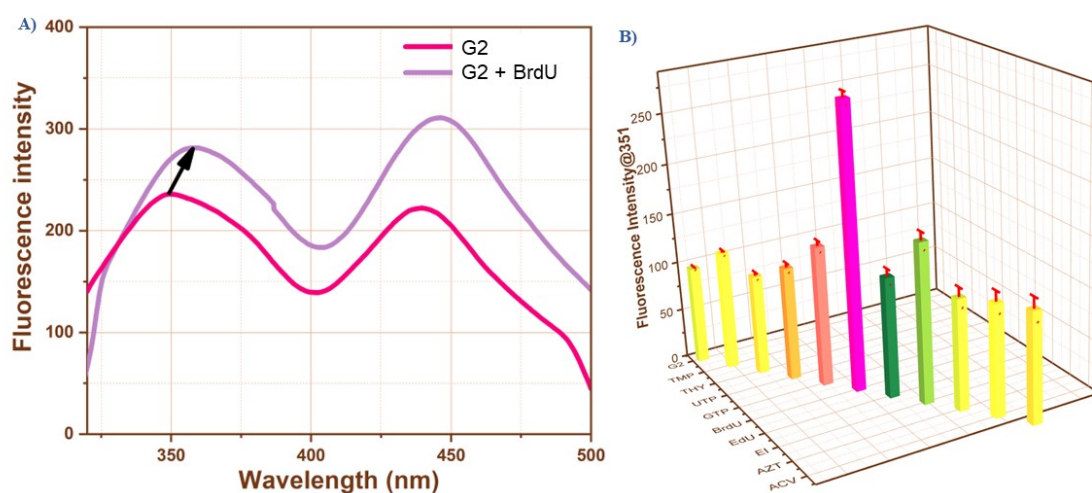


Fig. S8 A) Fluorescence spectrum showing shift and enhancement in emission intensity of **G2** upon addition of BrdU. B) Bar graph showing selectivity of **G2** towards BrdU.

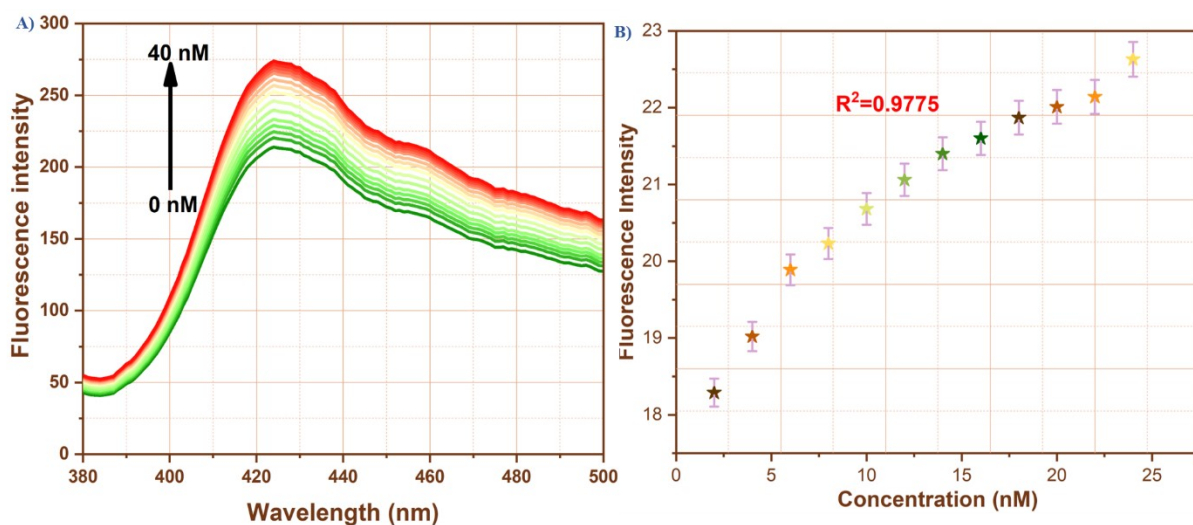


Fig. S9 A) Titrations of Ni complex in organic medium. B) Calibration plot of variation in fluorescence intensity on varying the concentration of BrdU.

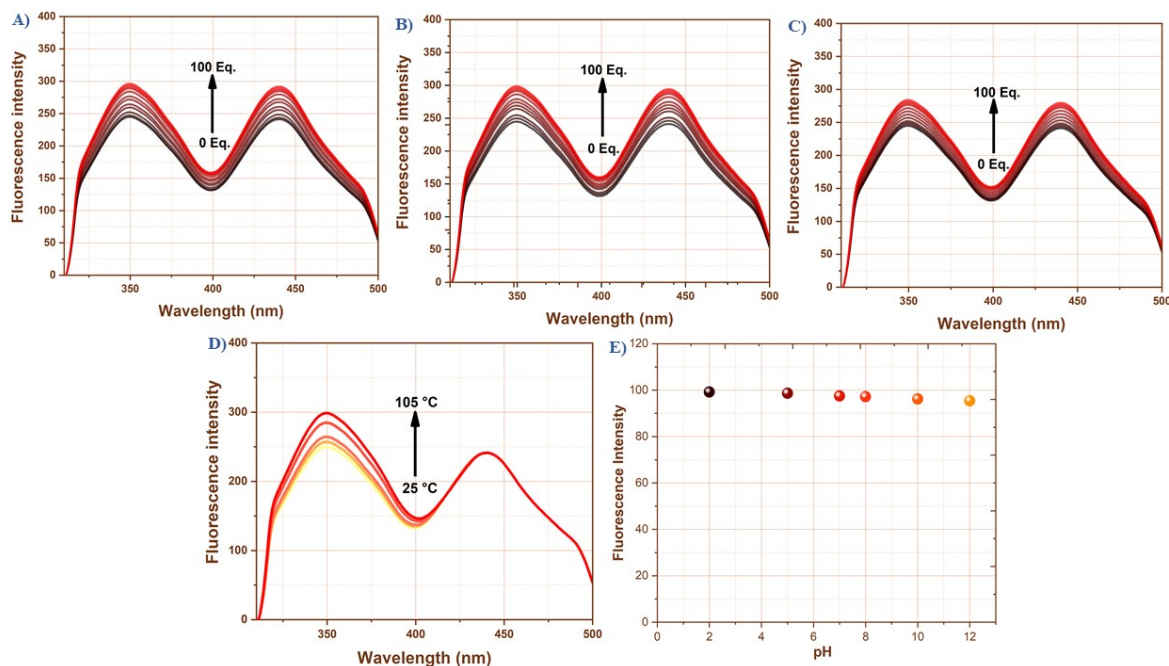


Fig. S10 Effect of tetrabutylammonium A) perchlorate B) phosphate C) sulphate, on the fluorescence emission intensity of **G2**. D) Effect of increase in temperature from 25-105 °C on fluorescence emission intensity of **G2**. E) Fluorescence spectrum showing negligible change in emission intensity of **G2** on varying pH from 2-12.

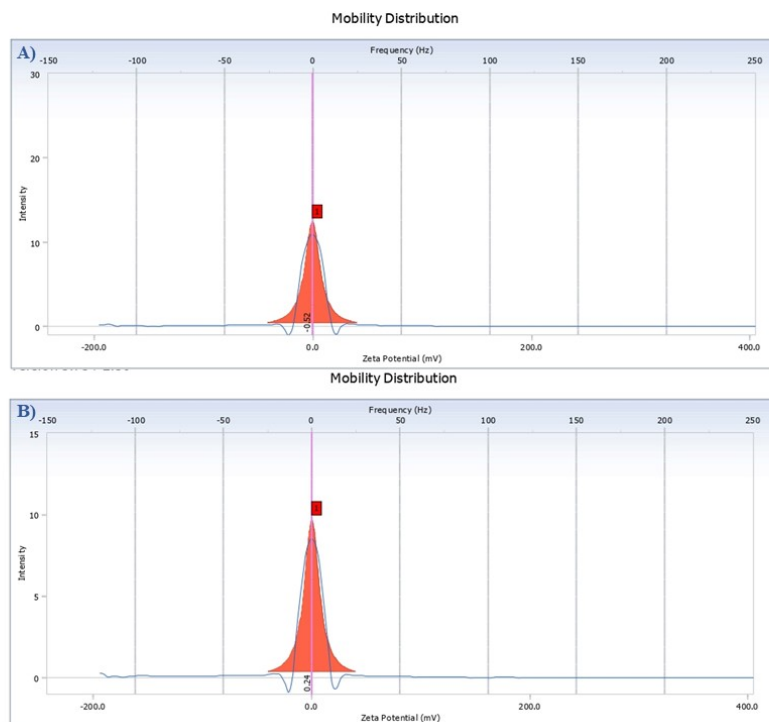


Fig. S11 Zeta potential of A) ONPs and B) Ni@G1 showing change in its surface charge upon coating.

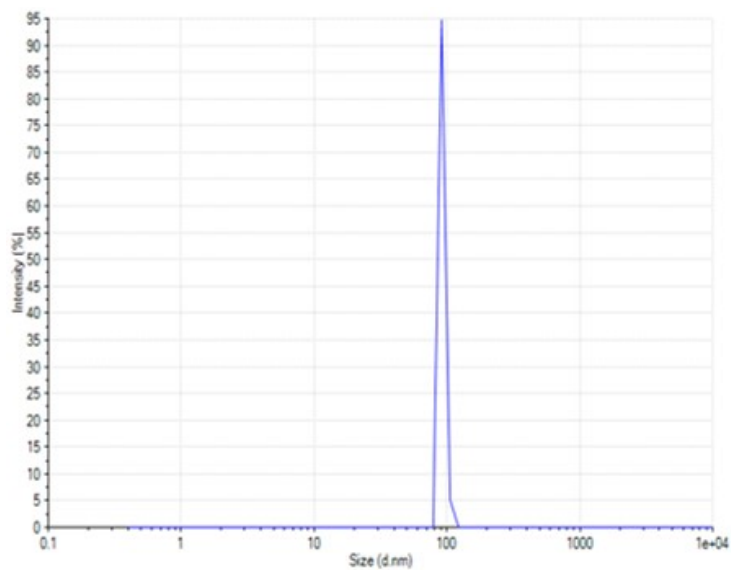


Fig. S12 DLS of Ni@G1 showing average hydrodynamic size of 92 nm.

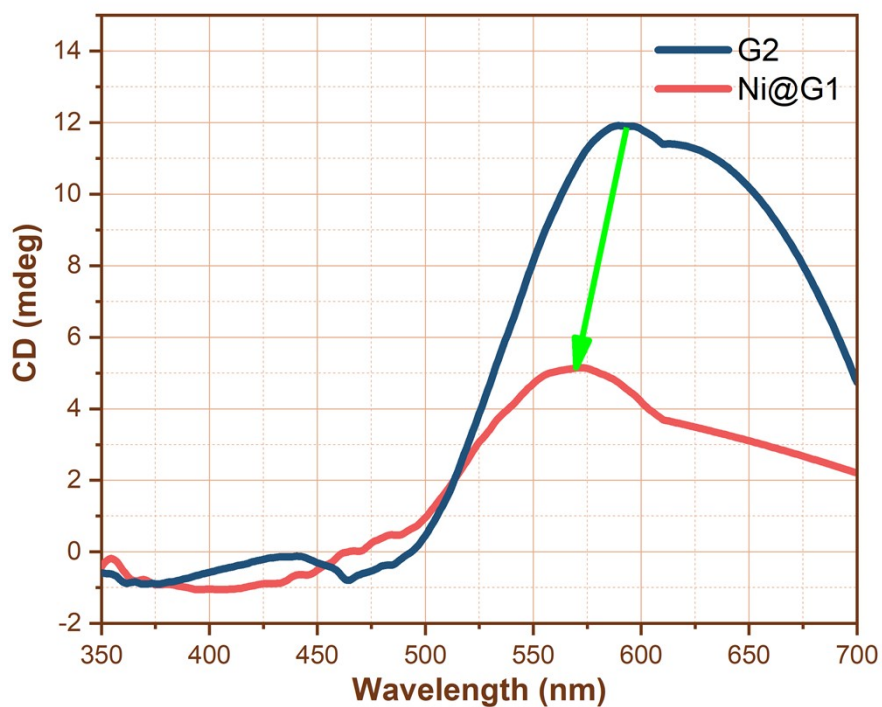


Fig. S13 A) Circular dichroism showing changes in ONPs profile upon formation of Ni@G1.

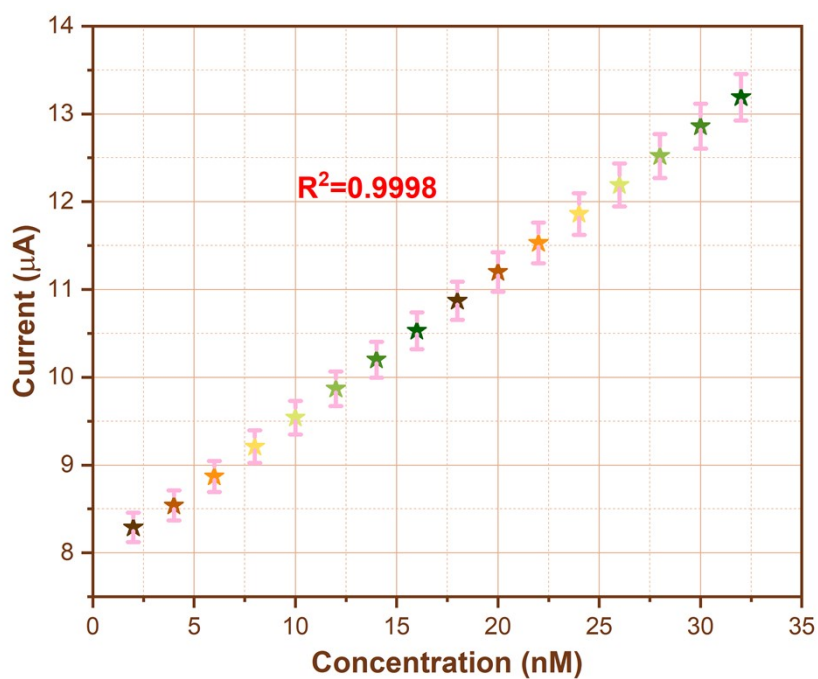


Fig. S14 Calibrations plot showing dependence of BrdU addition on Ni@G1 on Cyclic voltammetry.

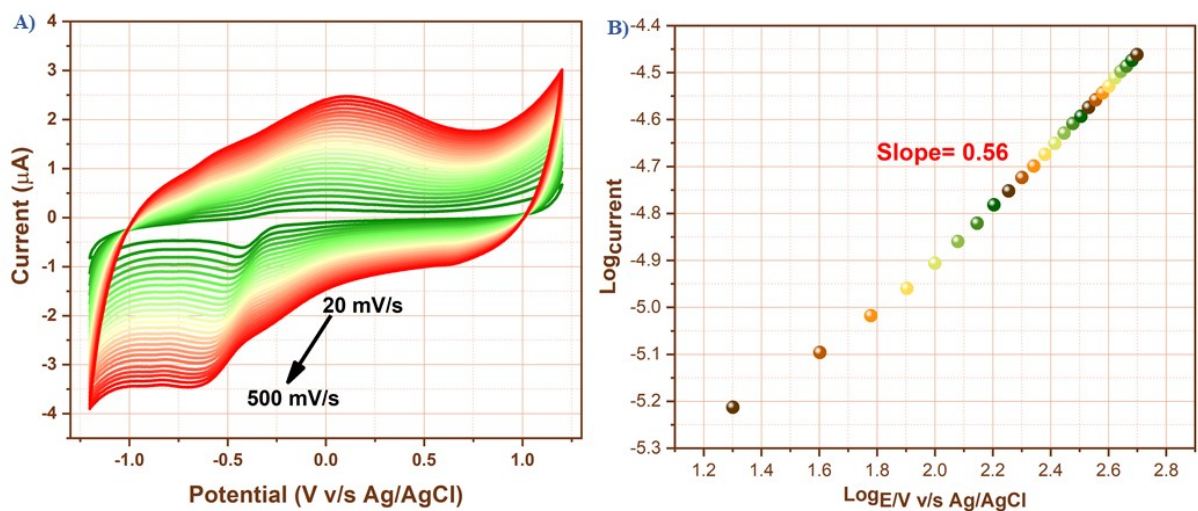


Fig. S15 A) Cyclic voltammogram showing variation in current and potential on varying scan rate from 20 – 500 mV/s. B) Linear regression plot between log current versus log of scan rate.

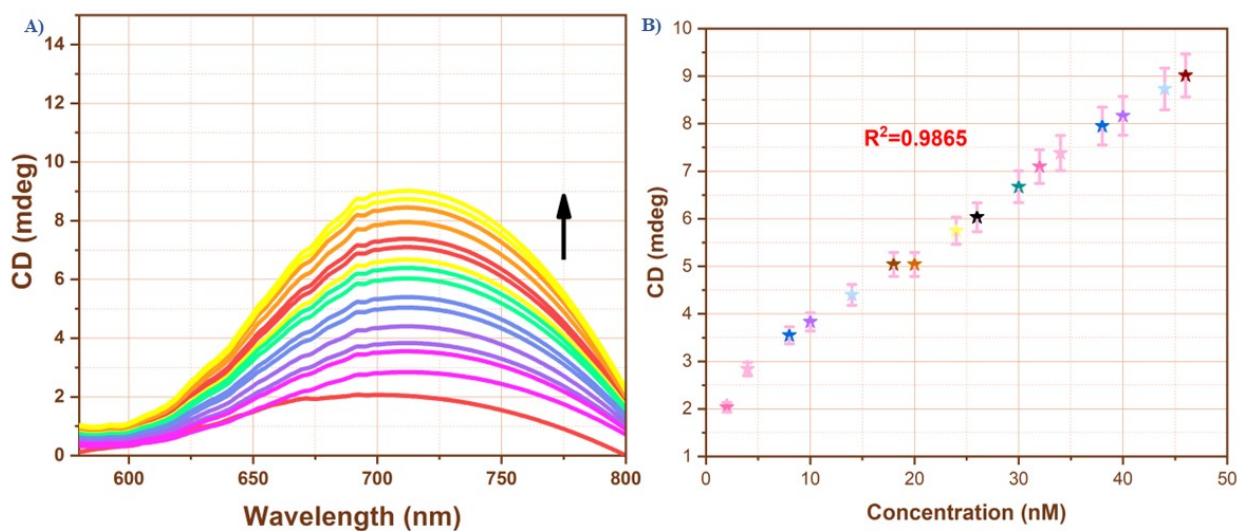


Fig. S16 A) Changes in dextrorotatory behavior on adding small aliquots of BrdU to Ni@G1. B) Calibration showing linearity of 98.65% with BrdU concentration.

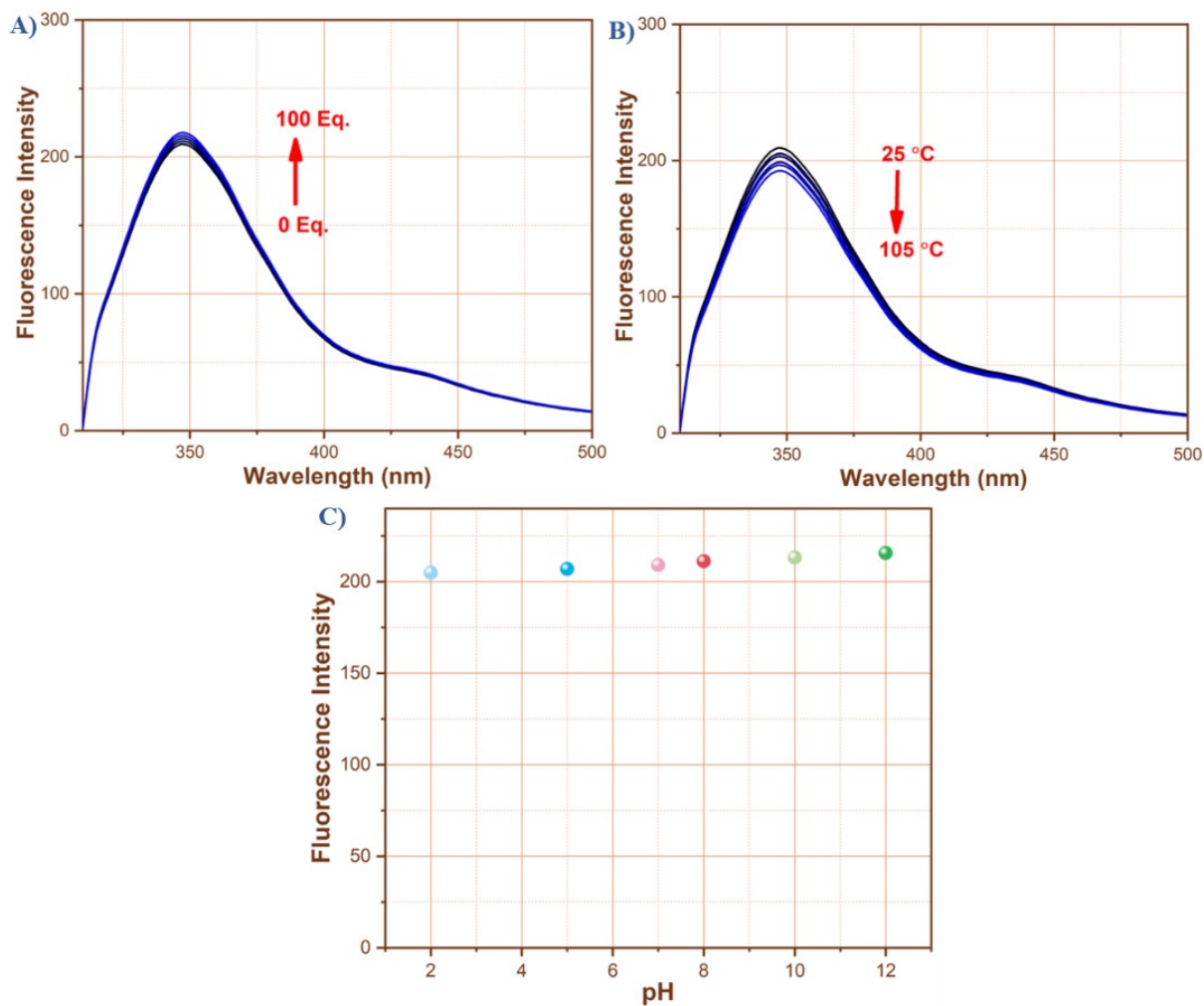


Fig. S17 A) Effect of tetrabutylammonium phosphate on the fluorescence emission intensity of Ni@G1 complexed with BrdU. B) Effect of temperature therapy from 25-105 °C on fluorescence emission intensity of Ni@G1 complexed with BrdU. C) Fluorescence spectrum showing negligible change in emission intensity of Ni@G1 complexed with BrdU on varying pH from 2-12.

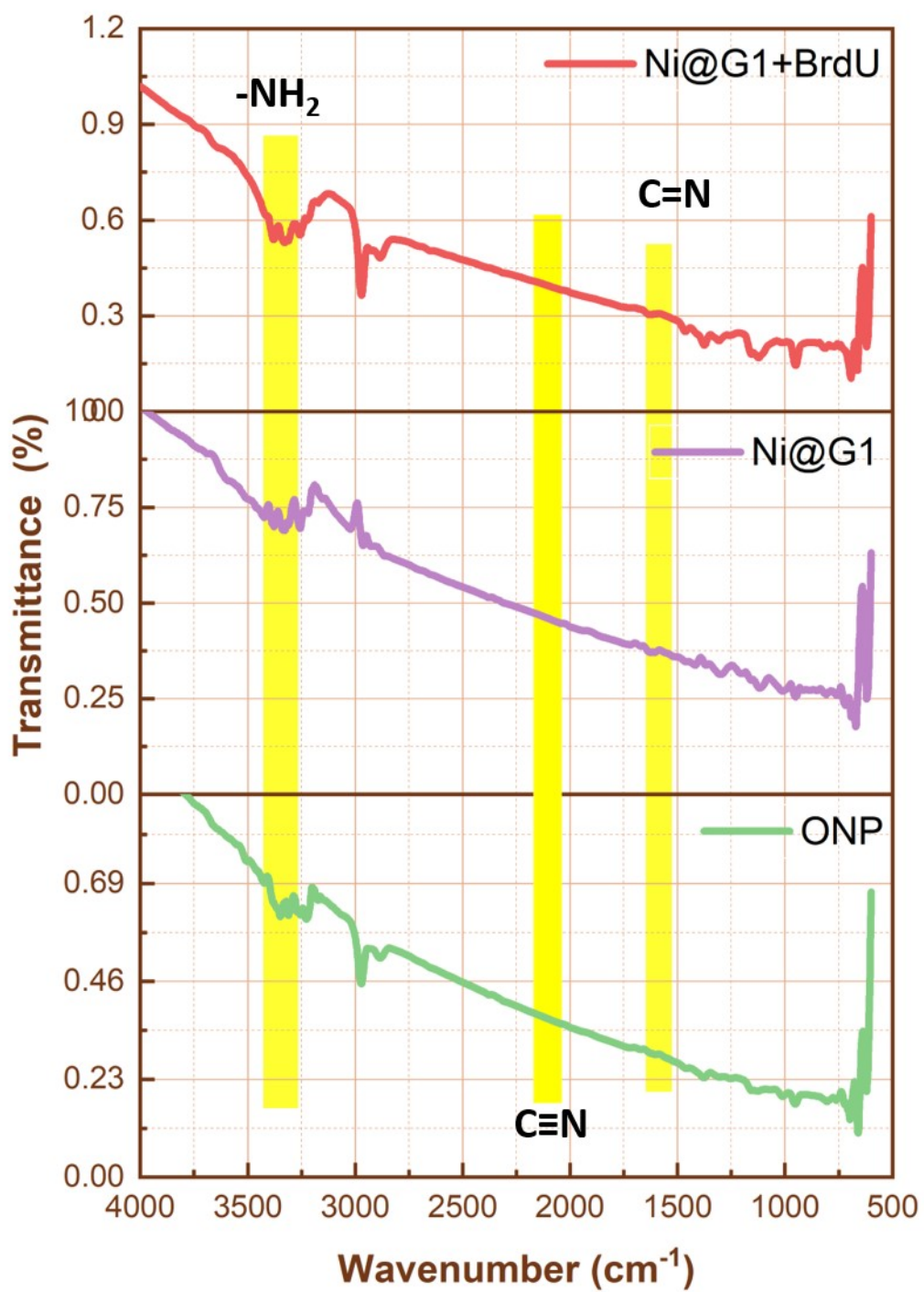


Fig. S18 FT-IR spectrum of ONP, Ni@G1, Ni@G1+BrdU.

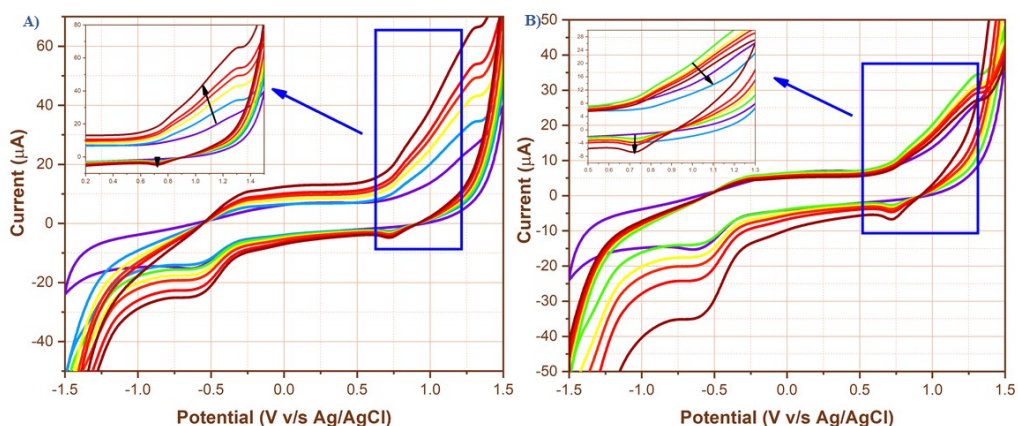


Fig. S19 A) Cyclic voltammogram showing changes in cathodic and anodic peak when Ni(II) is added to ONPs. B) Cyclic voltammogram when NaBH₄ is added to the **G2** complex formed.

S.No.	Compound	A ₁	τ _{AV}
1	Receptor G1	5339	3.99
2	ONPs	49075	0.23
3	G2	906.5	4.73
4	Ni@G1	3749.6	11.92

Table S1 Time resolved fluorescence data of receptor **G1**, ONPs, **G2** and Ni shell ONPs.

S.No.	Method used for Detection	Real sample application	Limitations	References
1	Flow cytometry	Rat blood serum	<ul style="list-style-type: none"> • Too slow • Expensive • Requires trained professional • Complex instrumentation 	1
2	Immunocytochemical detection	MCF-7 cells	The technique has some limitations: <ul style="list-style-type: none"> • Stains are not 	2

			<p>worldwide available</p> <ul style="list-style-type: none"> • Expensive instrument • Result quantification is difficult 	
3	Flow cytometry	Chinese hamster ovary cells	<ul style="list-style-type: none"> • Too slow • Expensive • Requires trained professional • Complex instrumentation 	3
4	Flow cytometry	<ul style="list-style-type: none"> • Keratinocytes • Bone marrow cells 	<ul style="list-style-type: none"> • Too slow • Expensive • Requires trained professional • Complex instrumentation 	4
5	Flow cytometry	<p>Cell lines including:</p> <ul style="list-style-type: none"> • Chinese hamster embryo cells • Human skin fibroblasts • Friend erythroleukemia cells 	<ul style="list-style-type: none"> • Too slow • Expensive • Requires trained professional • Complex instrumentation 	5

		<ul style="list-style-type: none"> Human lymphocytes 		
6	Immunocytochemical detection	Serum samples of: <ul style="list-style-type: none"> Canaries Quail Mice 	The technique has some limitations: <ul style="list-style-type: none"> Stains are not worldwide available Expensive instrument Result quantification is difficult 	6
7	High performance liquid chromatography (HPLC)	Human serum	The technique has some limitations: <ul style="list-style-type: none"> Costly Tedious Time consuming Complex 	7
8	Fluorescence spectroscopy, UV-Visible spectroscopy and Cyclic voltammetry	Human serum albumin	-----	Present work

Table S2 Comparison table of present work with other analytical techniques.

References

- 1 Z. Qiu, J. Shu and D. Tang, *Anal. Chem.*, 2017, **89**, 5152–5160.
- 2 F. Dolbeare, H. Gratzner, M. G. Pallavicini and J. W. Gray, *Proc. Natl. Acad. Sci. U. S. A.*, 1983, **80**, 5573–5577.

- 3 J. Van Heusden, P. De Jong, F. Ramaekers, H. Bruwiere, M. Borgers and G. Smets, *J. Histochem. Cytochem.*, 1997, **45**, 315–319.
- 4 P. E. J. Van Erp, P. P. T. Brons, J. B. M. Boezeman, G. J. De Jongh and F. W. Bauer, *Cytometry*, 1988, **9**, 627–630.
- 5 J. A. Steinkamp, 1987, 0–5.
- 6 J. M. Barker, T. D. Charlier, G. F. Ball and J. Balthazart, *PLoS One*, 2013, **8**, 1–5.
- 7 T. J. Kinsella, J. B. Mitchell, A. Russo, M. Aiken, G. Morstyn, S. M. Hsu, J. Rowland and E. Glatstein, *J. Clin. Oncol.*, 1984, **2**, 1144–1150.